Multicompartmental Microcapsules from Star Copolymer Micelles

ARTICLE *in* MACROMOLECULES · FEBRUARY 2013

Impact Factor: 5.8 · DOI: 10.1021/ma302483j

Macromolecules

Article

pubs.acs.org/Macromolecules

Multicompartmental Microcapsules from Star Copolymer Micelles

Ikjun Choi,[†] Sidney T. Malak,[†] Weinan Xu,[†] William T. Heller,[§] Constantinos Tsitsilianis,[‡] and Vladimir V. Tsukruk*,[†]

[†]School of Materials Science and Engineering, Georgia Institute of Technology, Atlanta, Georgia 30332-0245, United States

[‡]Department of Chemical Engineering, University of Patras, 26504 Patras, Greece, and Institute of Chemical Engineering and High Temperature Processes (FORTH/ICE-HT)

[§]Biology & Soft Matter Division, Oak Ridge National Laboratory, Oak Ridge, Tennessee 37831, United States

Supporting Information

ABSTRACT: We present the layer-by-layer (LbL) assembly of amphiphilic heteroarm pH-sensitive star-shaped polystyrene-poly(2-pyridine) (PS_nP2VP_n) block copolymers to fabricate porous and multicompartmental microcapsules. Pyridine-containing star molecules forming a hydrophobic core/hydrophilic corona unimolecular micelle in acidic solution (pH 3) were alternately deposited with oppositely charged linear sulfonated polystyrene (PSS), yielding microcapsules with LbL shells containing hydrophobic micelles. The surface morphology and internal nanopore structure of the hollow microcapsules were comparatively investigated for shells formed from star polymers with a different numbers of arms (9 versus 22) and varied shell thickness (5, 8, and 11 bilayers). The successful integration of star unimers into the LbL shells was demonstrated by probing their buildup, surface segregation behavior, and porosity. The larger arm star copolymer (22 arms) with stretched conformation showed a higher increment in shell thickness due to the effective ionic complexation whereas a compact, uniform grainy morphology was observed regardless of the number of deposition cycles and arm numbers. Small-angle neutron scattering (SANS) revealed that microcapsules with hydrophobic domains showed different fractal properties depending upon the number of bilayers with a surface fractal morphology observed for the thinnest shells and a mass fractal morphology for the completed shells formed with the larger number of bilayers. Moreover, SANS provides support for the presence of relatively large pores (about 25 nm across) for the thinnest shells as suggested from permeability experiments. The formation of robust microcapsules with nanoporous shells composed of a hydrophilic polyelectrolyte with a densely packed hydrophobic core based on star amphiphiles represents an intriguing and novel case of compartmentalized microcapsules with an ability to simultaneously store different hydrophilic, charged, and hydrophobic components within shells.

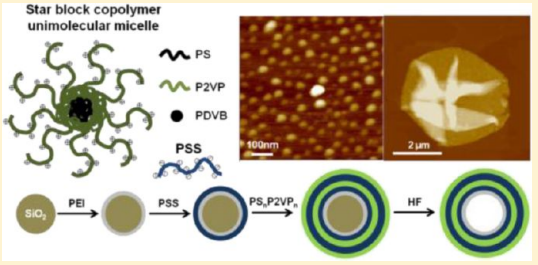

INTRODUCTION

Amphiphilic star block copolymers can be of great interest for use as a nanoscale container, catalyst, and template.[1−5] In particular, star polymers bearing polyelectrolyte arms might act as colloidal nanoparticles and offer a rich phase behavior under various environments.[6,7] The charged arms on the polyelectrolyte stars show stretched or retracted configuration depending upon an interplay of long-range electrostatic repulsion between arms and osmotic pressure induced by confined counterions. Such an effective interaction of soft-sphere colloids leads to dynamic response (e.g., arm collective relaxation and self-diffusion) by deformation and interdigitation.[8−11] At the surfaces and interfaces, highly branched star polymers adapt different conformations (e.g., spreading and extending) due to the steric repulsion between crowded chains.[12−14]

Typically, star polymers are comprised of multiple polymeric arms chemically grafted onto one core.[15] Star architecture including spherical topology, multiple valence of charge, and a terminal functional end group can be easily tailored by advanced synthetic methods.[16−29] The molecular organization of star polymers is similar to a spherical micelle of block copolymers with a thermodynamically frozen core, a polymer brush grafted onto spherical colloids, and hierarchical dendrimers. Star polymers are known to have a small aggregation number and a high critical micelle concentration (cmc) compared to corresponding linear analogues. The thermodynamically enhanced stability stemming from steric repulsion between crowding arms enables colloidal star polymers to exist in the form of a single molecule, so-called, "unimolecular micelle". Star block amphiphiles with pH-tunable multipolyelectrolyte arms have been shown to be a promising building component for responsive ultrathin films.[30−36] The sequential surface assembly of star polymers can offer a versatile strategy to fabricate nanofilms with well-defined composition and stratified compartments.[37,38]

Layer-by-layer (LbL) assembly using a planar or colloidal template substrate has been a useful means for preparing

Received: December 3, 2012
Published: February 6, 2013

   dx.doi.org/10.1021/ma302483j | Macromolecules 2013, 46, 1425−1436

Table 1. Molecular Characteristics of Heteroarm PS_nP2VP_n Star Block Copolymers

	no. of arms		PS_{arm}		$P2VP_{arm}$			
chemical structures	n	total	M_w	N_{PS}	M_w	N_{P2VP}	Φ_{P2VP}[a]	$M_{w,tot}$
PS_nP2VP_n	9	18	3400	33	13 200	126	0.80	149 000
	22	44	3500	34	14 300	136	0.80	386 000

[a]Weight fraction of P2VP.

tunable functional multilayer nanofilms, coatings, and membranes.[39] In particular, LbL hollow microcapsules assembled via electrostatic and/or hydrogen interactions create an alternately assembled multilayered shell wall and a hollow interior as a cargo carrier.[40,41] The permeability and pore structure of the microcapsules can be effectively tuned with a nanometer level accuracy by controlling the number of deposited layers and by an external field (e.g., pH, salinity, and temperature) due to the dynamically responsive and adaptive molecular transformations.

The dendrimers and linear block copolymers have been recently considered attractive building blocks for fabrication of functional LbL multilayer film and hollow microcapsules.[42] The ultrathin multilayers constructed from dendrimers have drawn a great deal of attention in drug delivery and sensor applications due to the polyvalency and controllable physicochemical properties of dendritic units.[43−45] The incorporation of dendrimers into multilayer shell wall can affect the capsule stability, permeability, and elasticity as compared to linear architecture polyelectrolytes. Khodade et al. reported high yield hollow capsules based on poly(amidoamine) dendrimers.[46,47] Kim et al. probed the mechanical property of phosphorus dendrimer/polyelectrolyte microcapsules and demonstrated softening and the enhanced permeability.[48,49]

On the other hand, the use of polymeric micelles based on amphiphilic linear block copolymers for the construction of hollow microcapsules has been reported.[50−57] For instance, Ma et al. prepared LbL microcapsules from polymer micelles and demonstrated the ability of loading−unloading behavior.[58,59] Biggs et al. presented a novel strategy to assemble micelle−micelle films and microcapsules using zwitterionic diblocks.[60,61] Hong et al. found that hairy micelles with long hydrophilic arms can be used to fabricate stable microcapsules.[62] The multiarm star polymers with their well-defined periphery arms can thus be considered as a promising candidate for the fabrication of functional microcapsules owing to their well-defined hierarchical characteristics.[63,64]

Here, we report on LbL microcapsules containing both pores and hydrophobic compartments in polyelectrolyte shells constructed from star-shaped heteroarm amphiphilic polystyrene-poly(2-pyridine) (PS_nP2VP_n) block copolymers (the subscript n denotes the number of arms (9 and 22 arms)). Specifically, the amphiphilic star coplymers with a high level of ionizable pyridine groups (Φ_{P2VP} = 80 wt %) were dispersed in an acidic aqueous environment, allowing for the formation of core/corona micelles. The core/corona star copolymers with protonated pyridine units, which are positively charged at pH 3, can be successfully assembled with negatively charged linear poly(styrenesulfonate) (PSS) to form stable microcapsules. The surface morphology of collapsed microcapsules clearly reveals that the star copolymers remain as a unimolecular micelle within the shell. Moreover, the combination of confocal laser scanning microscopy and small-angle neutron scattering (SANS) confirmed high porosity and fractal nature of these shells. Their enhanced colloidal stability and complex morphology of shells with nanopores and hydrophobic domains distributed in polyelectrolyte matrix facilitate the unique compartmental nature of these microcapsules that may enable controlled multicargo loading.

EXPERIMENTAL SECTION

Materials. Linear PSS (M_w = 70 kDa) and PEI (M_n = 10 kDa) from Aldrich were used as-received. 1.0 M TRIS HCl was purchased from Rockland and was diluted to 0.01 M in ultrapure pure water (Nanopure water with a resistivity of 18.2 MΩ cm) for use. 0.1 M HCl (99.5% purity) and 0.1 M NaOH (99.5%) solutions were utilized to adjust the pH of polyelectrolyte solutions. Fluorescence isothiocyanate (FITC) and FITC dextrans with different molecular weights were purchased from Sigma-Aldrich.

Synthesis of Star Block Copolymers. The amphiphilic heteroarm PS_nP2VP_n star block copolymers were synthesized by the "in−out method" via a multistep, one pot, and sequential anionic living polymerization route.[65,66] The first generation of PS arms was formed in the first step by using initiator, secondary butyl lithium (*sec*-BuLi) in tetrahydrofuran medium. Subsequently, these "living" linear PS chains were used to initiate the polymerization of divinylbenzene (DVB) acting as a multireactive cross-linker. A living PS star-shaped polymer was formed bearing an equal number of active sites within its polyDVB core with its PS arms followed by growth of the second generation of arms from the core upon the addition of 2-vinylpyridine (2VP). The conversion was monitored by sampling out the polymer solution. PS_nP2VP_n star copolymer was isolated and characterized. All samples were characterized by a combination of gel permeation chromatography, ^{1}H NMR, and light scattering in accordance with the approach published elsewhere and the results are summarized in Table 1.[66]

Substrate Preparation. Freshly cut silicon substrates with dimensions 1 cm × 2 cm and [100] orientation (Semiconductor Processing) and a native silicon dioxide layer having a 1.6 nm thickness were cleaned with piranha solution (3:1 concentrated sulfuric acid and hydrogen peroxide mixture) in accordance with usual procedure.[67] Subsequently, they were abundantly rinsed with Nanopure water and dried with a dry nitrogen stream. Pretreated substrates served as a hydrophilic planar substrate for film deposition.

Preparation of LbL Planar Film and Hollow Microcapsules. As summarized in Table 1, amphiphilic heteroarm PS_nP2VP_n star block copolymers with different number of arms (9 versus 22 arms) and molecular weights (149 000 versus 386 000 Da) were employed to fabricate LbL films. All monolayer and multilayer films and microcapsules were obtained by a dip-assisted LbL method. PS_nP2VP_n heteroarm star block copolymers were dispersed in 0.2 mg/mL concentration mixed solution (4.0 vol % of dimethyformamide (DMF) and 96 vol % of 0.01 M TrisHCl buffer solution) at pH 3 under sonication. The monolayer of PS_nP2VP_n star copolymer monolayer was deposited on a silicon substrate without a prelayer by a 15 min dipping followed by a 2 min washing in the same buffer solution. The PEI adhesive prelayer was used for all multilayer films. A polyanionic PSS layer was deposited first followed by polycationic PS_nP2VP_n star copolymer. The deposition cycle was repeated until the desired number of layers was obtained. The silicon substrate was placed in each polymer solution for 15 min followed by washing for 2 min in the same pH buffer solution. The monolayer and multilayer films were dried under mild nitrogen flow for ellipsometry and AFM measurement.

The PS_nP2VP_n/PSS LbL hollow microcapsules were prepared using silica microsphere core (4.0 ± 0.2 μm in diameter, 10% dispersions in water, Polyscience, Inc.) as a sacrificial template as illustrated in Figure

dx.doi.org/10.1021/ma302483j | Macromolecules 2013, 46, 1425−1436

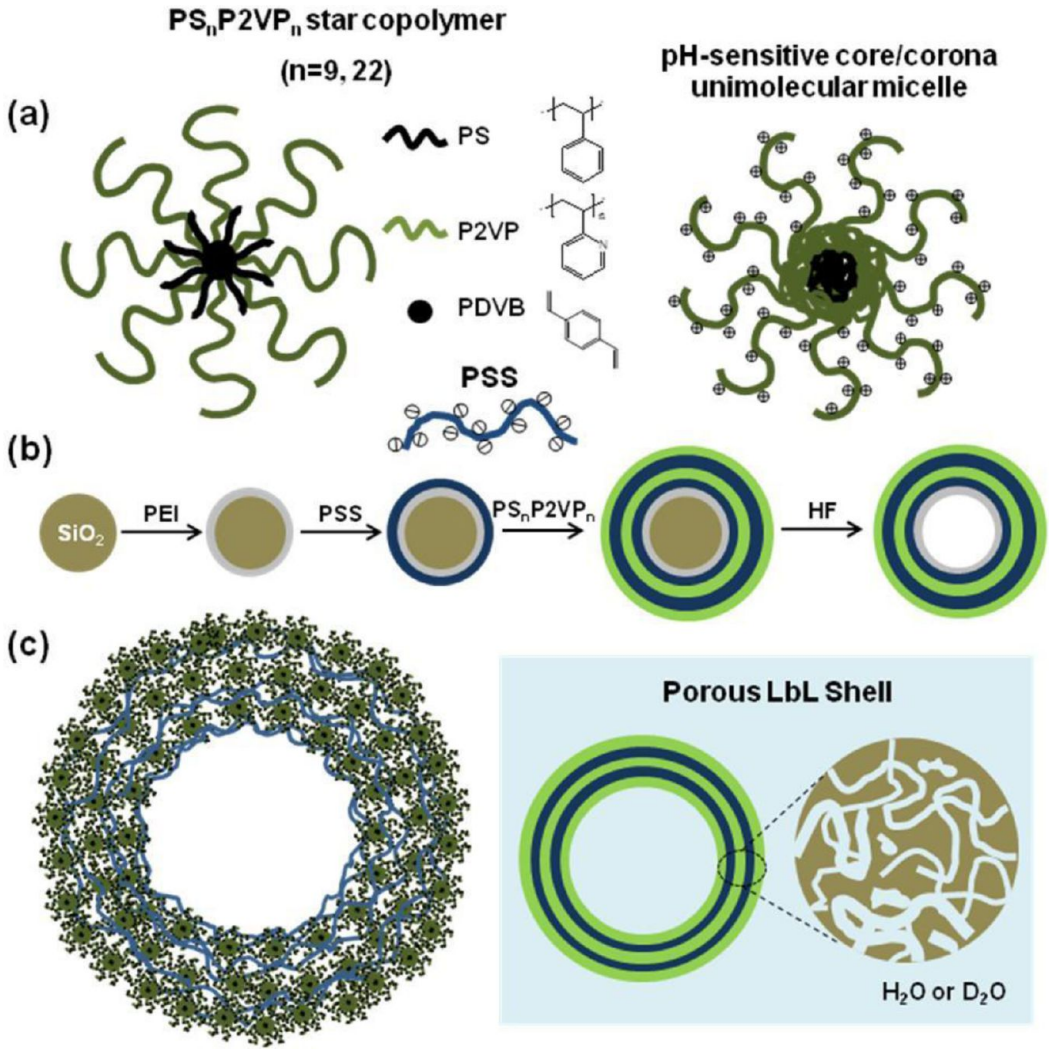

Figure 1. (a) Molecular structure and composition of amphiphilic heteroarm PS$_n$P2VP$_n$ star block copolymers (left) and their core/corona unimolecular micelles (right); (b) fabrication procedure and (c) multilayer structure of an assembled star polymer hollow microcapsule (left) and its corresponding porous shell morphology (right).

1b.[68,69] The silica cores were alternately immersed in 0.2 mg/mL polymer solution at pH 3 via repeated deposition cycles. The assembly of each polymer layer was conducted for 15 min with constant shaking. The microcapsules were precipitated by centrifugation at 2000 rpm for 2 min to separate solid and supernatant, and then the collected capsules were rinsed three times with 0.01 M TrisHCl buffer solution at the same pH. The assembly/washing cycle was repeated until a desirable thickness of the capsule was obtained. The silica cores were removed using diluted 0.2 M hydrofluoric acid (HF) at pH 3. To obtain hollow capsules, the core dissolution process was repeated three times to ensure that the silica core was completely removed. The capsules were isolated by centrifugation at 7000 rpm for 10 min, followed by three thorough washings with the same buffer solution. The core dissolution was confirmed by confocal microscopy and AFM.

Characterization of LbL Planar Film and Hollow Microcapsules. Measurement of film thicknesses and refractive indices were made with a Woollam M2000U (J.A. Woollam Co, Inc., Lincoln, NE) multiangle spectroscopic ellipsometer at three incident angles 65°, 70°, and 75°. The Ψ (polarized angle) and Δ (phase) values were measured and used in conjunction with a Cauchy model (WVASE32 analysis software) to determine the thickness of the LbL films and their optical constants n and k over the wavelength range 245−1000 nm.

The morphological properties of the LbL film and capsule surface were probed under ambient conditions in the tapping and phase modes in air and fluid with nanometer resolution using a Dimension 3000 (Veeco Inc., Santa Barbara, CA). For quantitative analysis of surface topography and roughness, AFM images were obtained in the "light" tapping mode with an amplitude ratio within 0.90−1.00 to avoid surface damage and film deformation.[70,71] The AFM cantilevers had spring constants in the range of 40−60 N/m. Scanning rates were between 1.0 and 2.0 Hz, depending on the scan area which ranged from 10 μm × 10 μm to 1 μm × 1 μm.[72]

Confocal images of LbL hollow microcapsules were acquired by a LSM 510 VLS META inverted confocal laser scanning microscope equipped with a 63 × 1.4 oil immersion objective lens (Zeiss). Excitation/emission wavelengths of 488/515 nm were used. A small volume of a dispersion of hollow capsules were placed into Lab-Tek chambers (Electron Microscopy Sciences) and then analyzed after they settled. To investigate capsule permeability to FITC-dextrans, hollow capsules were added to several Lab-Tek chambers, which were then half-filled and mixed with FITC-dextran solutions. To confirm the alternating assembly of polymer pairs on the silica core, the surface potentials were monitored on Zetasizer Nano-ZS equipment (Malvern). Each value of the zeta-potential was obtained at ambient conditions by averaging three independent measurements of 35 subruns each.

SANS Measurements. All samples were measured in D_2O to minimize the incoherent backscattering and increase contrast for hydrogenated shells.[73] For the 22-arm star polymer, the microcapsules

dx.doi.org/10.1021/ma302483j | Macromolecules 2013, 46, 1425−1436

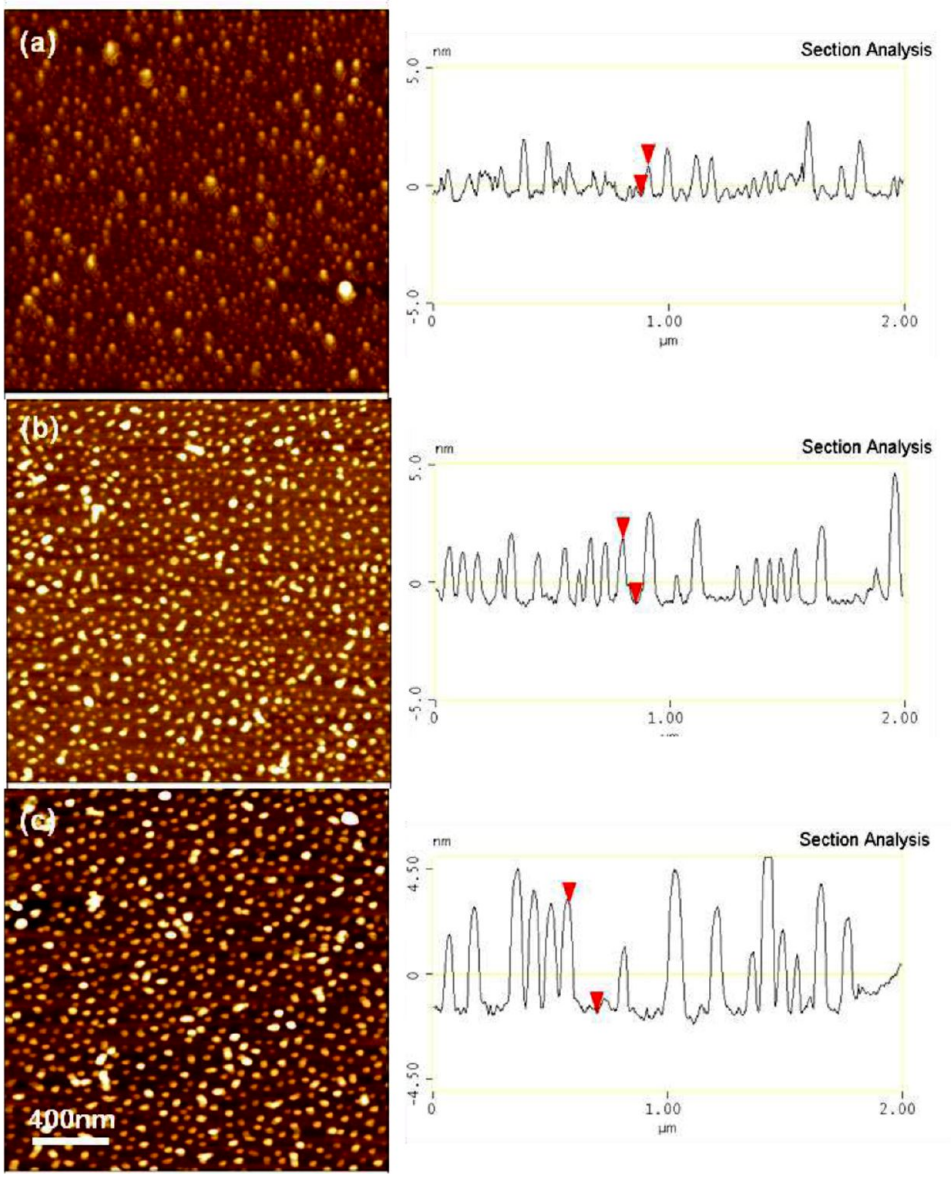

Figure 2. AFM topography image (left) and cross-sectional analysis (right) of PS_nP2VP_n star block copolymer monolayer on planar silicon substrate in dry state obtained by dip-assisted deposition method at pH 3. (a) PS_9P2VP_9 in 4% DMF mixed aqueous solution. (b) $PS_{22}P2VP_{22}$ in 4% DMF mixed aqueous solution. (c) $PS_{22}P2VP_{22}$ in 4% acetone mixed aqueous solution. The *z*-scale of all AFM images is 10 nm.

with different shell thickness (5, 8, and 11 bilayers) in hydrogenated water were treated with deuterated water (D_2O) that was adjusted to pH 3 using 0.1 M HCl. To minimize the mixing of H_2O, the D_2O exchange was repeated three times using the centrifugation method. The final capsule concentration was sufficiently dilute to minimize capsule−capsule scattering effects. This reduces the complexity of data fitting by eliminating the effects of a structure factor (i.e., $S(q) \approx 1$). Samples were loaded into 1 mm path length "banjo" style quartz cuvettes (Hellma USA, Plainview, NY). All SANS measurements were made at room temperature (22 °C) on the extended-Q small-angle neutron scattering (EQ-SANS) instrument of the Spallation Source at Oak Ridge National Lab (ORNL).[74]

The time-of-flight instrument was operated in 30 Hz (frame-skipping) mode using a minimum wavelength, λ, of 2.5 Å, yielding two bands of neutrons (2.5−6.1 and 9.4−13.4 Å). A sample-to-detector distance of 4 m was used, resulting in a q-range of approximately 0.0035−0.45 $Å^{-1}$, where "q" is the momentum transfer vector defined as $q = (4\pi/\lambda)\sin(\theta/2)$ and θ is the scattering angle, which probes dimensions on the order of 10−1500 Å (distance = $2\pi/q$). Data correction for proton charge normalization, wavelength-dependent flux and sample transmission, background, detector sensitivity, and instrument dark current (cosmic radiation and electronic noise) followed the standard procedures implemented in MantidPlot. Azimuthally averaged intensity profiles from the two neutron bands employed were merged using the routine implemented in MantidPlot. To convert the data into absolute units (1/cm), an absolute intensity calibration was conducted using a calibrated standard, which in this case was Porasil B in a 1 mm path length quartz cuvette.[75] Nonlinear fitting of experimental data was conducted using SANSView.

RESULTS AND DISCUSSION

Chemical Composition and Unimolecular Micelles. The heteroarm star block amphiphiles employed in this study are comprised of hydrophobic PS blocks and pH-sensitive ionizable P2VP blocks that both emanate from a common single junction (Figure 1). Because of the pH-induced ionization of pyridine moieties on the P2VP block arms (80 wt %), star copolymers can exist in the form of a core/corona state in acidic aqueous solution, analogous to the amphiphilic

dx.doi.org/10.1021/ma302483j | *Macromolecules* 2013, 46, 1425−1436

linear block copolymers with a thermodynamically frozen core. The dispersion of amphiphilic star copolymers in the aqueous environment was achieved by employing a DMF/water solvent mixture where the pH value was adjusted to be acidic (pH 3). The use of polar DMF, which is a good solvent for both PS and P2VP segments, allows star amphiphiles to be solubilized with a corona/corona chain conformation.

The transparency of the solution was maintained, indicating that there is no distinct large-scale aggregation due to the increased solubility of the protonated pyridine groups of P2VP segments at sufficiently lower pH ($pK_{a,P2VP} \sim 4.3$).[76] Since the value of pK_a is defined as the pH when 50% neutralization of total ionic monomer units occurs in a titration curve, the extent of ionization can be estimated to be around 25% at pH 3 according to the literature.[50,64] Above pH 4.5 the solution becomes dramatically clouded because of the loss of hydrophilicity of pyridine units induced by their deprotonation. The solubility parameter (9.9 $(cal/cm^3)^{1/2}$) of P2VP at a un-ionized state is close to organic solvents such as chloroform (9.33) and tetrahydrofuran (9.51).[77]

Zeta-potential measurements show the apparent reduction in the electric potential of the polymer solution to be near pH 4.5, which is in good agreement with the observed change in the transparency at the same pH condition (Figure S1). However, the zeta-potential of star copolymer micelles shows the maximum positive value at pH 2, which could be presumably due to different surface charge contribution from the outer and inner ionic groups along the star polymer branch arms in contrast to solid nanoparticles. Since the zeta-potential is measured from the electrophoretic mobility and depends on the charges on the particle surface as well as the particle radius through, it is not easy to correlate the zeta-potential with the degree of ionization (pK_a). The colloidal stability of star polymer dispersant remains without pronounced precipitation over the long term. The multiarm molecular conformation of star polymers provides a favorable colloidal stability owing to the steric repulsion of a dense chain structure. Therefore, the dispersed star copolymers take the form of a collapsed hydrophobic PS core which is screened by a positively charged stretched P2VP corona (Figure 1a).[63,77]

The association of amphiphilic heteroarm star copolymers with long chain polyelectrolyte depends on the preparation method, the number of arms, the hydrophobic content, and the concentration (cmc). A $PS(3K)_{20}P2VP(23K)_{20}$ star prepared from a common good solvent forms unimolecular micelles in acidic aqueous solution due to the stabilization efficiency of the 20 polyelectrolyte arms.[64] Similarly, a $PS(20K)_7P2VP(56.5K)_7$ star with higher hydrophobic content was shown to exist as a unimer in very dilute solutions while it forms multimolecular micelles of low aggregation number (3−4) at higher concentration.[63] For the PS_9P2VP_9, which is similar to $PS(3K)_{20}P2VP(23K)_{20}$, some association that could lead to micelles comprising few stars (ca. 2 or 3) cannot be excluded. However, because the PS_9P2VP_9 poses much less hydrophobic content with respect to $PS(20K)_7P2VP(56.5K)_7$, we assume that this star mainly stays as unimer micelles. These assumptions are corroborated from the fact that no turbidity or bluish tint (evidence of association) was observed after the slow addition of acidic water.

Planar Film Morphology. The planar LbL films possess a discrete spherical domain structure displaying collapsed circular molecular conformation in the dried state (Figure 2). A densely packed monolayer with a uniform size distribution is revealed from the high-resolution AFM image in Figure 3. It is apparent that the size of aggregates depends on the number arms and the solvent, as illustrated by domain dimension results by AFM sectional analysis (Table 2). The 22-arm star polymers show larger domain height (2.4 ± 0.6 nm) than the 9-arm star polymer (1.5 ± 0.5 nm). A similar trend is observed with the domain width results (9 arms: 49.5 ± 6.0; 22 arms: 54.0 ± 5.7 nm). Moreover, such aggregation appears to depend on the solvent as seen from the different domain height for acetone and DMF, where the acetone mixture leads to slightly more swollen aggregation. This result is presumably due to the lower solubility of PS segments in acetone, leading to a larger aggregation number. In addition, the aggregation dimensional analysis and the uniform surface morphology of the monolayer suggest that star polymers remain as a unimicellar state. This is particularly true for the star polymer with 22 arms owing to the enhanced steric stabilization effect, even at relatively high concentration (0.3 mg/mL).[77]

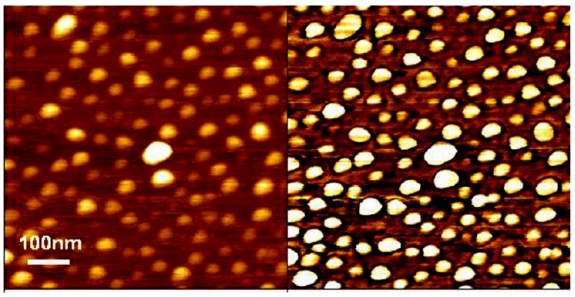

Figure 3. High-resolution AFM topography (left) and phase (right) image of $PS_{22}P2VP_{22}$ star block copolymer unimolecular micelles on planar silicon substrate in dry state deposited by the dip-assisted LbL method at pH 3. The *z*-scale is 10 nm (topography) and 60° (phase).

Table 2. Domain Height and Width of Star Copolymer Monolayer Films[a]

system	domain height (nm)	domain width (nm)
9 arms, DMF	1.5 ± 0.5	49.5 ± 6.0
22 arms, DMF	2.4 ± 0.6	54.0 ± 5.7
22 arms, acetone	3.3 ± 0.6	67.7 ± 5.6

[a]All data were determined from cross-section analysis of AFM topography images (2 μm × 2 μm) for dried samples. Tip dilation effect is responsible for excessive domain width with actual values being approximately 50% lower.

The growth behavior of LbL multiayers on a planar substrate was investigated using a dip-assisted LbL method to examine the first (Figure 4). Both 9-arm and 22-arm star copolymers were found to build up uniform films with the increase in the number of bilayers (1, 3, 5, 8, and 11 bilayers) when sequentially assembled with PSS at pH 3. This linear growth behavior is an indication of strong electrostatic attraction of positively charged pyridium groups on P2VP with oppositely charged sulfonate groups on PSS.[78] Table S1 shows the average bilayer thickness for LbL films, in particular that the bilayer thickness is 5.0 ± 0.4 nm in the case of 9 arms while 5.8 ± 0.2 nm for 22 arms. The 22-arm star polymer appears to enable faster growth of multilayer LbL films than the 9-arm star polymer. This result is likely due to the difference in domain size for different arm numbers, as demonstrated by the arm dependency on their monolayer structure (Figure 2). The

dx.doi.org/10.1021/ma302483j | Macromolecules 2013, 46, 1425−1436

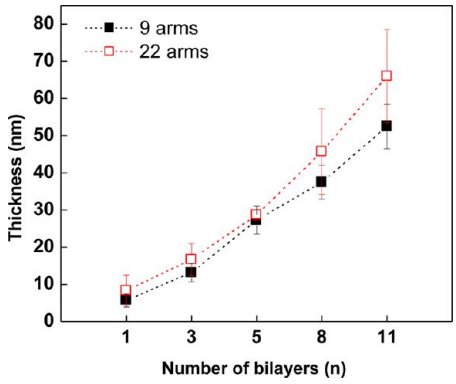

Figure 4. Buildup of PS_nP2VP_n/PSS LbL film on planar silicon substrate (9 arms (■) and 22 arms (□)).

greater number of arms appears to have an advantage to form ionic bonds, which can be attributed to more stretched chain conformation of the arms due to the steric constrains. Further, the polyvalent binding of the multiarm star architecture with higher number of arms is likely due to the large molecular weight, which is similarly to the case of larger molecular weight linear polyelectroytes.[79]

To probe the fine morphology of LbL films, high-resolution AFM topography images were collected for a varying number of bilayers (5, 8, and 11 bilayers), as displayed in Figure 5. The

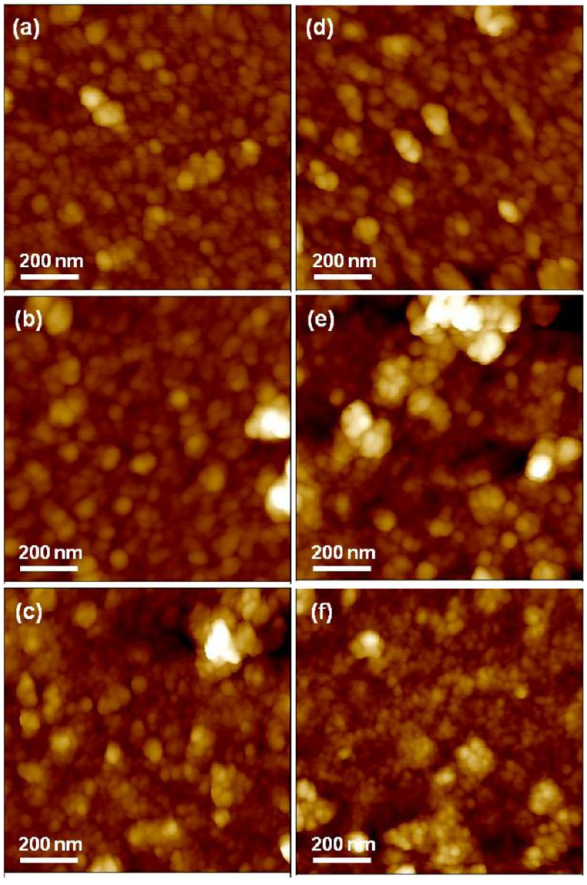

Figure 5. (a) AFM topography images of PS_nP2VP_n/PSS LbL multilayer film as a function of number of bilayers (5 (a, d), 8 (b, e), and 11 (c, f) bilayers) on planar silicon substrate in dry state (n = 9 arms (a–c) and 22 arms (d–f)). The z-scale is 120 nm.

spherical aggregate structure is clearly observed for films with different numbers of layers, where an increase in the number of bilayers appears to lead to larger size aggregates. In the case of the 9-arm star copolymer, the domain size is observed to be similar to that of the 22-arm star copolymer. The multiarm star copolymers seem likely to maintain stable micellar structures inside LbL multilayers after multiple deposition cycles. This observation implies the possibility to create a robust homogeneous multilayer assembly with discrete domain compartments based on star block copolymers.

Hollow Microcapsule Assembly and Shell Characteristics. The zeta-potential measurement displayed in Figure 6

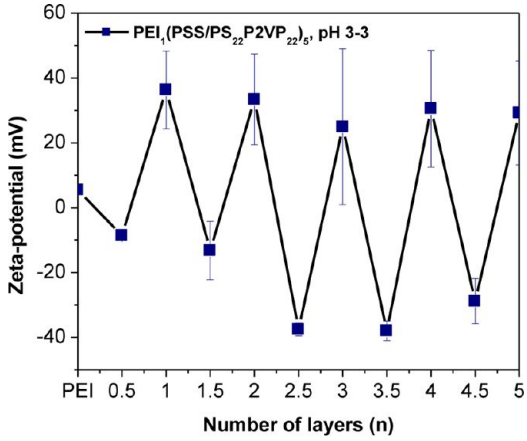

Figure 6. Zeta-potential measurements of $PS_{22}P2VP_{22}$/PSS LbL assemblies deposited on SiO_2 template core at pH 3.

proves that the polyelectrolyte pair undergoes a successive charge reversal and overcompensation during sequential multilayer buildup, thus indicating regular assembly on silica microparticles.

Upon core dissolution intact hollow microcapsule can be successfully obtained as demonstrated by the CLSM microscopy images (Figure S2 and Figure 7). Distinct size reduction of whole microcapsules after dissolution of cores was observed regardless number of arms. For five bilayer shells, the capsule shrinkage appears prominent (50% reduction in diameter) with several wrinkles becoming visible (Figure S3). However, with increase in the number of bilayers (up to 50 nm in shell thickness), the microcapsule diameter is stabilized (less than 15% reduction) because of uniform shells are formed.

Indeed, for 5 and 8 bilayers, the microcapsules were found to have a prominent buckled wall structure, which appears to be similar to the deformation of PSS/PDADMAC shells.[80] The degree of buckling appears to be decreased for thicker shells (Figure S2 and Figure 7). This tendency of buckling is analogous to thin film on the patterned substrates and on cores.[81−83] The possible driving force of the shrinkage of hollow capsules is the increased hydrophobic interaction in predominantly hydrophilic shells.[84,85] Upon compensation of cationically charged ionized pyridium on P2VP with anionic PSS counterpart, uncharged P2VP seems to no longer contribute for the solubilization of star polymers. Such additional hydrophobic interactions can lead to the reduced surface tension at water/polyelectrolyte interface.

In order to further elucidate the shell morphology, the AFM images were collected for collapsed microcapsule walls (Figure 8). For both 9-arm and 22-arm star polymers, the number of

dx.doi.org/10.1021/ma302483j | Macromolecules 2013, 46, 1425−1436

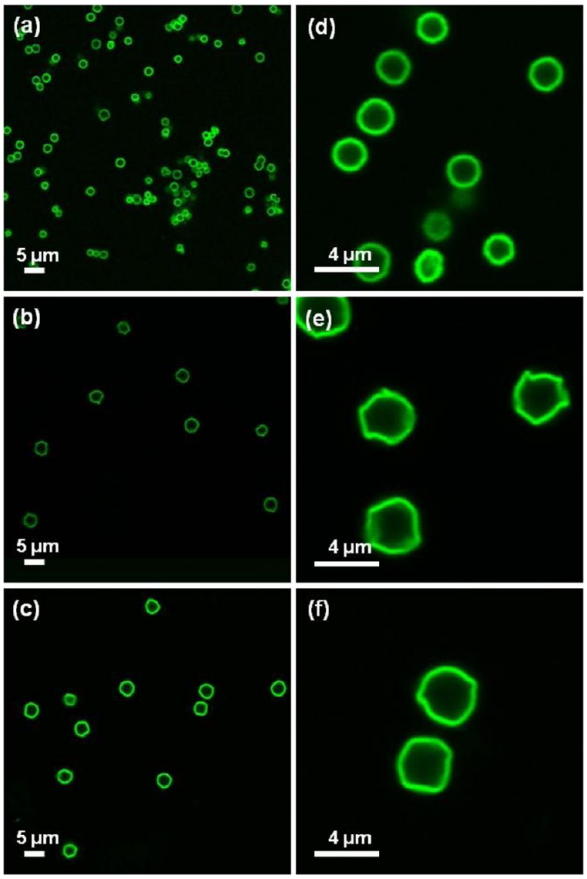

Figure 7. CLSM images (lower resolution (a–c) and higher resolution (d–f)) of $PS_{22}P2VP_{22}$/PSS microcapsules as a function of number of bilayers (5 (a, d), 8 (b, e), and 11 (c, f)).

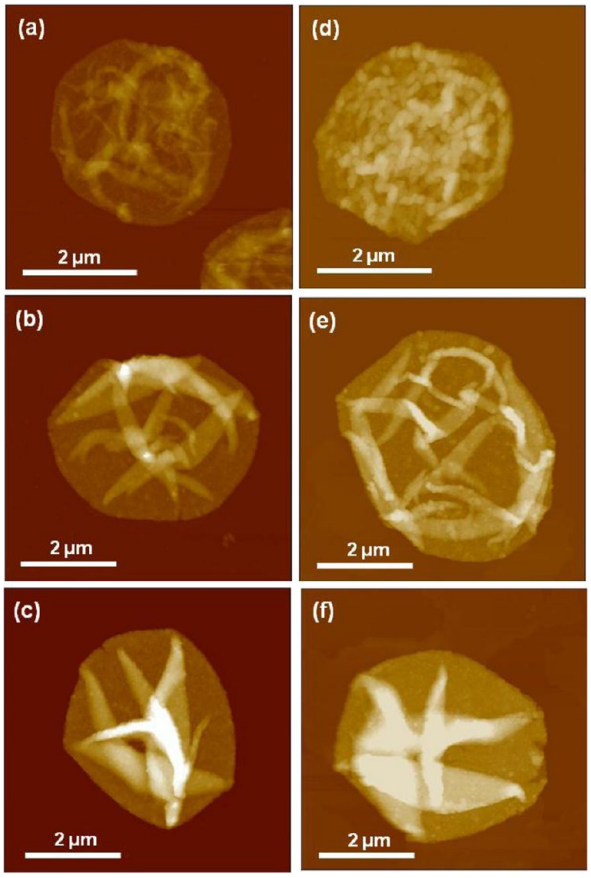

Figure 8. AFM topography images of PS_nP2VP_n/PSS microcapsules (9 arms (a–c) and 22 arms (d–f)) as a function of number of bilayers (5 (a, d), 8 (b, e), and 11 (c, f) bilayers) on silicon substrate in the dry state. The *z*-scale of all images is 600 nm.

wrinkles appears to be reduced, whereas more pronounced folded structures were observed as the film thickness increases. These results suggest that the increased shell thickness leads to the formation of more rigid films and, thus, allows for being persistent against capillary deformation during the drying process. The stable microcapsules were obtained irrespective of number of arms, but a similar trend in the folding phenomena was observed as illustrated in Figure S4. However, the microcapsules composed of 9-arm star copolymer showed thinner shells as expected due to the difference in molecular weights as discussed above for planar films (Figure 9a and Table S1).[79] The thickness of microcapsules was found to be lower than that of planar film, which is attributable to fabrication process during the capsule assembling.[86] The overall morphology of microcapsules is relatively smooth and indicates modest aggregation (microroughness of 3–8 nm) (Figure 9b).

The high-resolution AFM topography images (1×1 μm) of the microcapsules composed of 22-arm star block copolymer show the uniform surface morphology of shells with compact spherical domains (Figure 10). Regardless of change in the number of deposition layers, the similar grainy morphology as that typically seen in the dried collapsed LbL microcapsules with weak interaction of components.[79,87,88] The aggregate dimensions remain to be close to the ones of the unimolecular star copolymer monolayers (Figure S5). These results confirm that star polymers can exist as a single molecular micelle without undergoing large-scale microphase separation. This enhanced colloidal stability of multiarm star polymers can be ascribed to the multivalent arms in contrast to the case of dendrimers or conventional micelles.[47,60,62,89]

Figure 11 shows the thickness change and surface morphology for rehydrated microcapsules composed of 22-arm star block copolymers. The liquid AFM scan was performed to probe shell swelling properties. The swelling ratio was determined from measuring the difference in thickness between dried and rehydrated capsule shells. The rehydrated microcapsules under liquid cell setup with filled with the pH 3 Tris buffer solutions of 0.01 M concentration are found to swell up to on average 8% and reveal that the smooth surface morphology due to the highly hydrated surface in contrast to the granular texture of the dry shell. Notably, the low increment in the shell thickness in the wet state suggests that the capsules assembled from strong electrolyte at low ionic strength (0.01 M) stay neutral due to the high charge compensation and strong ionic bonding, leading to hydrophobic shell with the low level of free ionic groups.[90–92]

Porosity of LbL Shells. In order to probe the porous structure of the microcapsules as a function of deposited number of bilayers, measurements of the permeability were conducted using fluorescence dye labeled dextran with varying molecular weights, which correspond to the pore size of the shell.[93] Figure 12 depicts the CLSM images of microcapsules placed in solutions with different dextrans labeled with FITC dye. High contrast (no interior fluorescence) indicates nonpermeable shell state and permeation results in uniform fluorescence. Table 3 summarizes the permeability behavior

dx.doi.org/10.1021/ma302483j | *Macromolecules* 2013, 46, 1425–1436

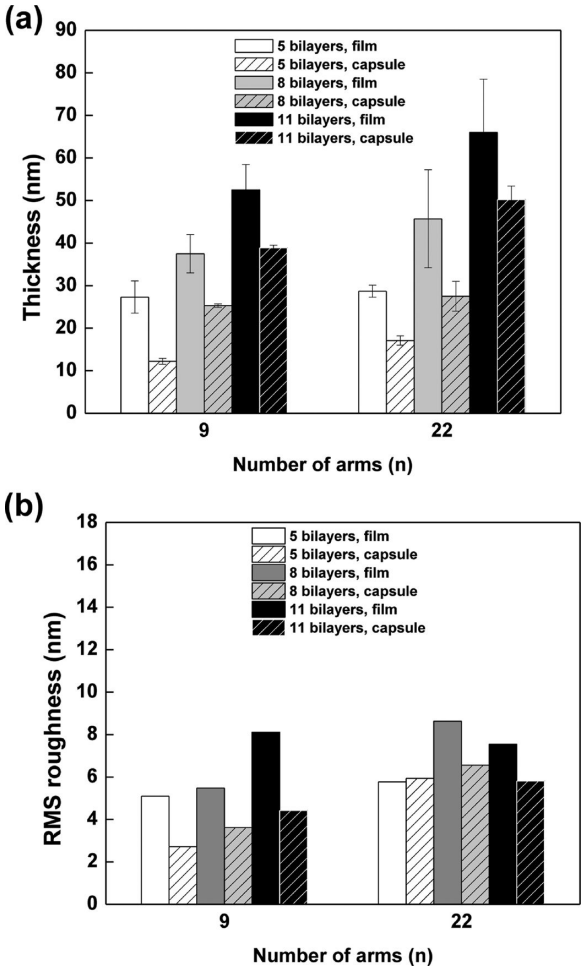

Figure 9. (a) Thickness and (b) rms roughness of dried shell wall of PS_nP2VP_n/PSS microcapsules for different bilayers (5, 8, and 11 bilayers) compared to those of corresponding films on planar silicon substrate.

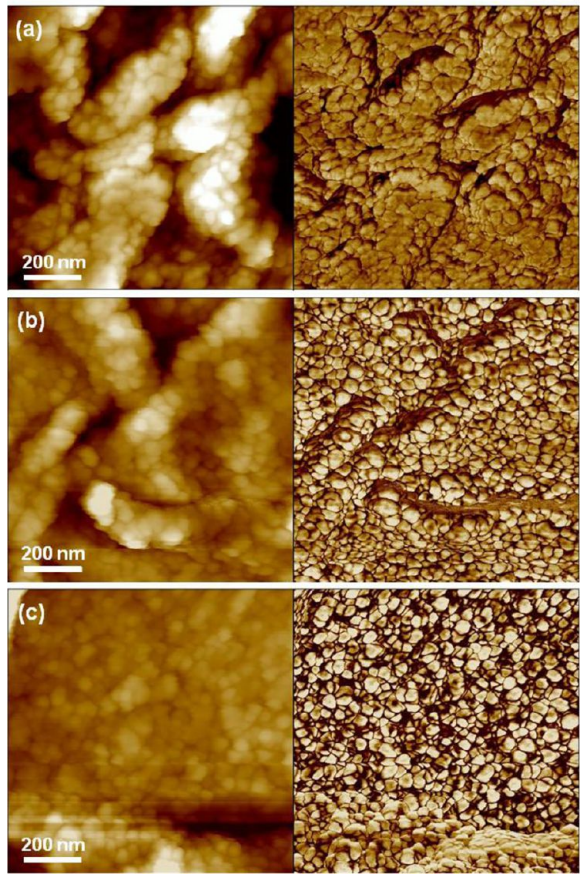

Figure 10. High-resolution AFM images (topography (left) and phase (right)) of $PS_{22}P2VP_{22}$/PSS microcapsules as a function of number of bilayers (5 (a), 8 (b), and 11 (c) bilayers) on silicon substrate in dry state. The *z*-scale of all images is 120 nm (topography) and 30° (phase).

found for the 22-arm star copolymer microcapsules and demonstrates the ability to tailor its permeability by varying the number of deposition layers. Either permeable or nonpermeable state for dextrans with different molecular weights can be achieved by changing the shell thickness. The five bilayer microcapsules appear to be a complete permeable while the microcapsule show reduced permeability against the larger molecular weight dextran (Table 3). In striking contrast, the 9-arm star copolymer microcapsules are highly permeable regardless of the number of deposition layers which indicates less dense, open porous structure with larger pore dimensions even for thicker shells.

The pore dimensions estimated from hydrodynamic diameter of permeating dextran macromolecules correspond to the value of around 23 nm for thicker shells.[94] The pores stay larger than 35 nm for the thinnest shells and for all microcapsules fabricated from 9-arm star copolymer. However, although the estimation of the pore dimensions from permeability experiments is popular, in fact, it is coarse and does not provide comprehensive information on true pore shapes, their distribution, and intrinsic morphology.

Therefore, in order to elucidate the porous morphology of the shells, SANS measurements were conducted for the deuterated water (D_2O) solutions. Here, we report SANS results on microcapsules made from the 22-arm star copolymer since the microcapsules from the 9-arm star copolymer do not show a high enough contrast for these experiments.

A significant increase in neutron scattering was observed for all microcapsules in a *q*-range of 0.04−0.5 nm^{-1} (Figure 13a). The scattering intensity increases with an increase in the number of bilayers, indicating that the scattering is directly related to the volume fraction of shells in the deuterated solution. The crossover between the 8- and 11-bilayer scattering curves at 0.07 nm^{-1} could be due to a general decrease in the 11-bilayer scattering intensity due to the solution having a lower concentration than the 5- and 8-bilayer microcapsule solutions. This reduction in intensity does not affect the data fitting since it affects the entire scattering curve and is simply a scale factor for the intensity.

It is important to note that the *q*-range for the scattering effects in this experiment corresponds to distances of 1−100 nm, which includes all the characteristic dimensions of several important structural features of our microcapsules known from independent measurements: total thickness of shells within 30−50 nm, domains size within 20−30 nm, and pore dimensions around 20 nm. However, considering the differences in scattering densities and the fact that deuterated water can readily diffuse into hydrogenated shells, we can suggest that the scattering contrast is highest between pores filled with deuterated water and the hydrogenated shell material while the contrast within hydrogenated material is much lower. Therefore, we suggest that the scattering in this region is likely

dx.doi.org/10.1021/ma302483j | *Macromolecules* 2013, 46, 1425−1436

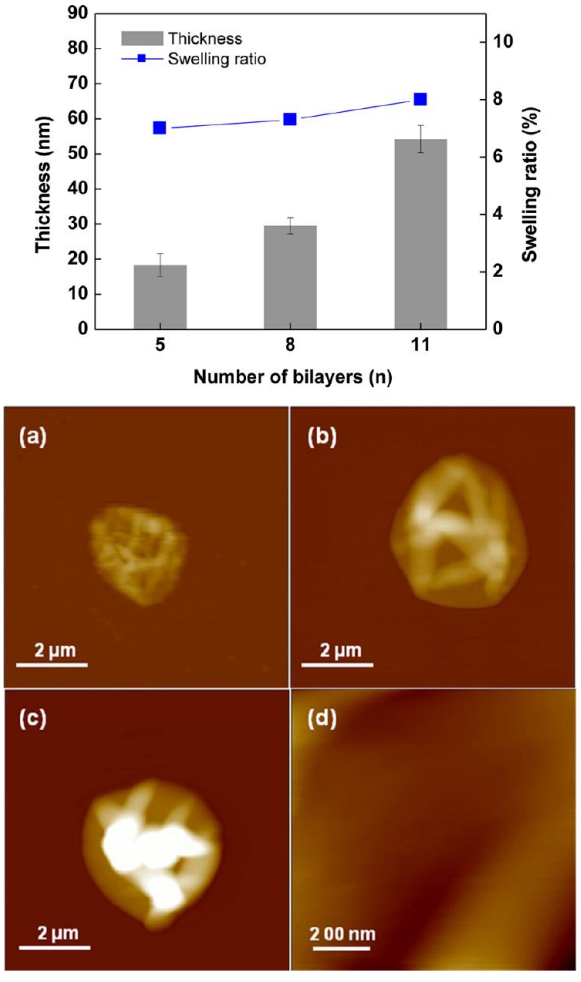

Figure 11. (top) Shell thickness and swelling ratio and (bottom) AFM images of rehydrated $PS_{22}P2VP_{22}$/PSS LbL hollow microcapsules as a function of number of bilayers (5 (a), 8 (b), and 11 (c) bilayers) and (d) high-resolution image of the surface of capsule (c) using liquid cell scan under pH 3 Tris buffer of 0.01 M. The *z*-scale of the images is 600 nm for (a–c) and 120 nm for (d).

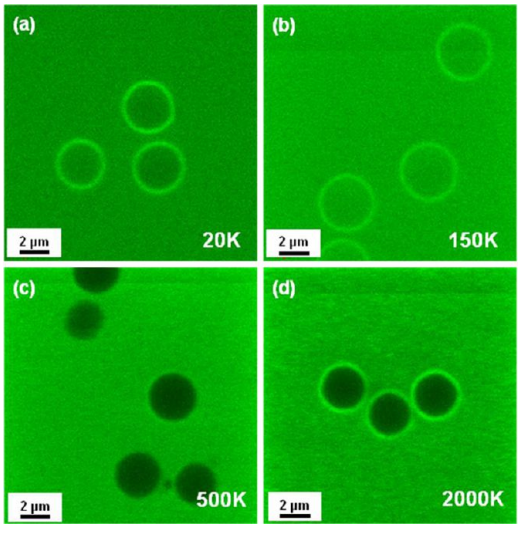

Figure 12. CLSM images of $PS_{22}P2VP_{22}$/PSS microcapsules (11 bilayers) using FITC-labeled dextran with varying molecular weights (Da): (a) 20 000, (b) 150 000, (c) 500 000, and (d) 2 000 000.

Table 3. Permeability of $PS_{22}P2VP_{22}$/PSS Microcapsules[a]

	dextran				
system	20 kDa	150 kDa	250 kDa	500 kDa	2000 kDa
PEI(PSS/$PS_{22}P2VP_{22}$)$_5$	+	+	+	+	+
PEI(PSS/$PS_{22}P2VP_{22}$)$_8$	+	+	±	−	−
PEI(PSS/$PS_{22}P2VP_{22}$)$_{11}$	+	+	±	−	−

[a]Fluorescein isothiocyanate (FITC)-labeled dextrans with different molecular weights (kDa). "+" permeable, "±" partially permeable, and "−" nonpermeable.

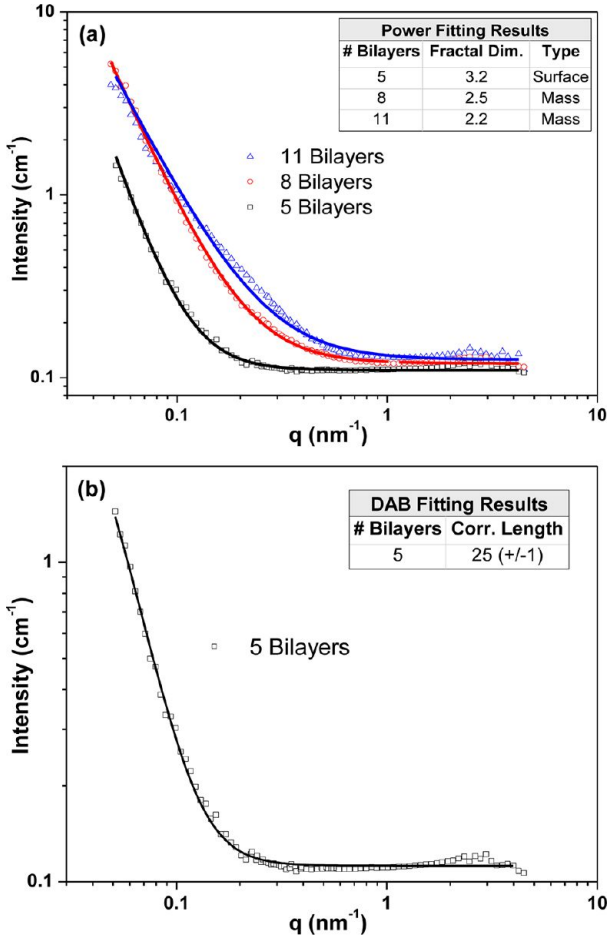

Figure 13. SANS data of fully hydrated $PS_{22}P2VP_{22}$/PSS microcapsules with (a) (square) 5 bilayers, (circle) 8 bilayers, and (triangle) 11 bilayers in D_2O solution that have been fitted with a power law model to determine the evolution of the fractal dimension and (b) the 5-bilayer sample with a DAB fit.

dominated by the pores with the lower *q* contribution coming also from the shell thickness.

Nonlinear fitting analysis was applied to the scattering data to confirm the trends observed for capsule thickness and the pore size dimensions as measured independently. In order to analyze scattering data, first, we suggested that the pores could be represented by individual objects with the scattering contrast determined by the hydrogenated polymer media and the pure deuterated water in the pores. In this analysis we varied the pore shape, their dimensions, and their polydispersity in attempts to fit experimental data. However, no such model provided satisfactory data fits. Therefore, the model of shell

dx.doi.org/10.1021/ma302483j | *Macromolecules* 2013, 46, 1425–1436

morphologies with distributed, individual, and well-defined closed pores can be excluded from further consideration.

Second, two shape-independent models which are based upon the representation of scattering media as highly randomized interconnected morphologies with diffuse contributions of weakly contrasted inhomogeneities at multiple length scales were applied to determine general trends. Initially, the scattering data were fitted with a power law model to determine the fractal dimension of randomized, network-like morphologies (Figure 13a).[95,96] In contrast to the model of individual scattering elements, the power law model yielded a good fit for the data sets over their entire q-range for all microcapsules studied here (Figure 13a). The fractal dimensions for each system determined from this analysis are shown in the inset of Figure 13a.

Importantly, significant differences in power law fits were observed for microcapsules with different shell thickness. The 5-bilayer microcapsules show a fractal dimension of 3.2, which strongly suggests a surface fractal morphology, i.e., a rough and highly folded uneven surface. This fractal distribution correlates well with the models of polymer distribution under modestly favorable adsorption conditions for LbL films with a limited number of layers as has been directly observed in AFM studies.[97] In contrast, the shells with an increased number of bilayers (8 and 11 bilayers) have a significantly reduced fractal dimension of 2.5 and 2.2, respectively, which suggests a mass fractal structure. Such a model corresponds to a network-like porous morphology with network elements randomly distributed within the shell (Figure 1c). This combination is likely indicative of a denser system which can be approximated by a randomly clustered network with major elements of high contrast formed by the swollen hydrogenated polyelectrolyte matrix and the nanopores filled with deuterated water.

Such a transition from the surface fractal to the mass fractal for shell thickness increasing from 5 to 8 bilayers revealed here corresponds to general trends in morphological changes with the increasing number of layers as suggested based upon microscopic observations.[97−99] The gradual filling of the initial two-dimensional network by subsequent polymer layers results in the formation of more uniform films with diminishing through-pores and decreasing pore dimensions. The occurrence of such reorganization is also supported by the results from fluorescence microscopy and AFM that are discussed above which demonstrate a densification of the surface morphology and a consistent decrease in the permeability. Moreover, significant shrinkage of microcapsules with only a few bilayers can be naturally related to the initial open surface network formation followed by collapse during core removal.

Finally, another model for multilength scale random morphologies, the Debye−Anderson−Brumberger (DAB) model, was also used to determine a correlation length in spatial distribution of density inhomogeneities within the shells (Figure 13b).[100] The DAB model assumes that the scattering objects have random sizes and shapes and show an exponentially decaying correlation in their spatial distribution.[101] Initial results show that the DAB model fits the 5-bilayer data quite well over the entire q-range and provides a correlation length of about 25 nm which can be interpreted as the characteristic dimension of density inhomogeneities represented by pores. It is worth it to note that this value is very close to that estimated from the dextran permeability measurements that additionally facilitate our interpretation of the SANS data. However, the DAB model does not properly describe the data from the thicker shell capsules, which presumably have smaller pore dimensions and denser shells contributing to the scattering in this q-range, likely because the assumptions regarding random pore sizes, shapes, and distributions are less accurate. Although these fitting results are preliminary and do not provide specific geometrical information on the capsule pores, they have provided an initial foundation for additional studies. Future investigation of pore geometries in these star polymer LBL microcapsules will be targeted toward capsules that have a large difference in size between microcapsule wall thickness and pore size. This design will make it possible to clearly isolate the scattering from each of these structures which will allow for more reliable fitting with the shape-dependent models.

CONCLUSIONS

In summary, we have demonstrated that the star copolymer unimolecular micelles can be successfully utilized to form unique multicompartamental LbL microcapsules with shells of coexisted network-like morphology of hydrophobic domains, hydrophilic polyelectrolyte matrix, and nanoscale water-filled pores. Such a unique shell morphology of thin-shell microcapsules might facilitate the ability for concurrent storage of hydrophobic, hydrophilic, and charged species in different compartments of shells based upon highly branched block copolymer macromolecules. The buildup of such microcapsules is controlled by star copolymer architecture with the enhanced hydrophobic characteristics and is efficient for star copolymers with a larger number of arms. We suggest that highly branched star copolymers maintain a core/shell unimolecular micelle within the shell with a granular morphology while effectively contributing to the buildup of stable multilayer shells with a complex network-like morphology. The polyvalent strong electrostatic interaction of core/corona multiarm architecture enables spherical star micelles to be incorporated into microcapsules with the ability to control shell morphology and the porous network structure.

ASSOCIATED CONTENT

Supporting Information

Table S1 and Figures S1−S5. This material is available free of charge via the Internet at http://pubs.acs.org.

AUTHOR INFORMATION

Corresponding Author

*E-mail vladimir@mse.gatech.edu.

Notes

The authors declare no competing financial interest.

ACKNOWLEDGMENTS

This work is supported by Grant NSF-DMR 1002810. The authors thank K. Campbell, O. Shchepelina, D. Kulkarni, Z. Combs, and C. Ye for technical assistance. The authors are thankful to Dr. N. Kroger for providing instrumentation for zeta-potential measurements. This research at ORNL Spallation Neutron Source was sponsored by the DOE Office of Basic Energy Sciences.

REFERENCES

(1) Gao, H. *Macromol. Rapid Commun.* **2012**, *33*, 722.
(2) Elsabahy, M.; Wooley, K. L. *Chem. Soc. Rev.* **2012**, *41*, 2545.
(3) Liu, X.; Jin, X.; Ma, P. X. *Nat. Mater.* **2011**, *10*, 398.

(4) Lee, V. Y.; Havenstrite, K.; Tjio, M.; McNeil, M.; Blau, H. M.; Miller, R. D.; Sly, J. *Adv. Mater.* **2011**, *23*, 4509.
(5) Barreto, J. A.; O'Malley, W.; Kubeil, M.; Graham, B.; Stephan, H.; Spiccia, L. *Adv. Mater.* **2011**, *23*, H18.
(6) Likos, C. N.; Löwen, H.; Watzlawek, M.; Abbas, B.; Jucknishke, O.; Allgaier, J.; Richter, D. *Phys. Rev. Lett.* **1998**, *20*, 4450.
(7) Jusufi, A.; Likos, C. N.; Löwen, H. *Phys. Rev. Lett.* **2002**, *88*, 018301−1.
(8) Vlassopoulos, D. *J. Polym. Sci., Part B: Polym. Phys.* **2004**, *42*, 2931.
(9) Jusufi, A.; Likos, C. N.; Ballauff, M. *Colloid Polym. Sci.* **2004**, *282*, 910.
(10) Shusharina, N. P.; Rubinstein, M. *Macromolecules* **2008**, *41*, 203.
(11) Rud, O. V.; Mercurieva, A. A.; Leermakers, F. A. M.; Birshtein, T. M. *Macromolecules* **2012**, *45*, 2145.
(12) Sheiko, S.; Sun, F. C.; Randall, A.; Shirvanyants, D.; Rubinstein, M.; Lee, H.-I.; Matyjaszewski, K. *Nature* **2006**, *440*, 191.
(13) Panyukov, S.; Sheiko, S. S.; Rubinstein, M. *Phys. Rev. Lett.* **2009**, *102*, 148301−1.
(14) Spatz, J. P.; Eibeck, P.; Mössmer, S.; Möller, M.; Kramarenko, E. Y.; Khalatur, P. G.; Potemkin, I. I.; Khokhlov, A. R.; Winkler, R. G.; Reineker, P. *Macromolecules* **2000**, *33*, 150.
(15) Pelelshanko, S.; Tsukruk, V. V. *Prog. Polym. Sci.* **2008**, *33*, 523.
(16) Kanaoka, S.; Omura, T.; Sawamoto, M.; Higashimura, T. *Macromolecules* **1992**, *25*, 6407.
(17) Voulgaris, D.; Tsitsilianis, C.; Esselink, F. J.; Hadziioannou, G. *Polymer* **1998**, *39*, 6429.
(18) Tsitsilianis, C.; Voulgaris, D. *Macromol. Rep.* **1995**, *A32*, 569.
(19) Ge, Z.; Xu, J.; Wu, D.; Narain, R.; Liu, S. *Macromol. Chem. Phys.* **2008**, *209*, 754.
(20) Peleshanko, S.; Gunawidjaja, R.; Jeong, J.; Shevchenko, V. V.; Tsukruk, V. V. *Langmuir* **2004**, *20*, 9423.
(21) Peleshanko, S.; Jeong, J.; Gunawidjaja, R.; Tsukruk, V. V. *Macromolecules* **2004**, *37*, 6511.
(22) Peleshanko, S.; Jeong, J.; Shevchenko, V. V.; Genson, K. L.; Pikus, Yu.; Petrash, S.; Tsukruk, V. V. *Macromolecules* **2004**, *37*, 7497.
(23) Gunawidjaja, R.; Peleshanko, S.; Tsukruk, V. V. *Macromolecules* **2005**, *38*, 8765.
(24) Genson, K. L.; Hoffman, J.; Teng, J.; Zubarev, E. R.; Vaknin, D.; Tsukruk, V. V. *Langmuir* **2004**, *20*, 9044.
(25) Gunawidjaja, R.; Peleshanko, S.; Kirsten, L. G.; Tsitsilianis, C.; Tsukruk, V. V. *Langmuir* **2006**, *22*, 6168.
(26) Voulgaris, D.; Tsitsilianis, C. *Macromol. Chem. Phys.* **2001**, *202*, 3284.
(27) Iatridi, Z.; Roiter, Y.; Stavrouli, N.; Minko, S.; Tsitsilianis, C. *Polym. Chem.* **2011**, *2*, 2037.
(28) Choi, I.; Gunawidjaja, R.; Suntivich, R.; Tsitsilianis, C.; Tsukruk, V. V. *Macromolecules* **2010**, *43*, 6818.
(29) Hammond, M. R.; Li, C.; Tsitsilianis, C.; Mezzenga, R. *Soft Matter* **2009**, *5*, 2371.
(30) Pitsikalis, M.; Pispas, S.; Mays, J. W.; Hadjichristidis, N. *Adv. Polym. Sci.* **1998**, *135*, 1.
(31) Hadjichristidis, N. *J. Polym. Sci., Part A: Polym. Chem.* **1999**, *37*, 857.
(32) Beyer, F. L.; Gido, S. P.; Poulos, Y.; Avgeropoulos, A.; Hadjichristidis, N. *Macromolecules* **1997**, *30*, 2373.
(33) Beyer, F.; Gido, S. P.; Uhrig, D.; Mays, J. W.; Tan, N. B.; Trevino, S. F. *J. Polym. Sci., Part B: Polym. Phys.* **1999**, *37*, 3392.
(34) Grayer, V.; Dormidontova, E.; Hadziioannou, G.; Tsitsilianis, C. *Macromolecules* **2000**, *33*, 6330.
(35) Iatridi, Z.; Tsitsilianis, C. *Chem. Commun.* **2011**, *47*, 5560.
(36) Iatridi, Z.; Tsitsilianis, C. *Polymers* **2011**, *3*, 1911.
(37) Tsukruk, V. V.; Rinderspacher, F.; Bliznyuk, V. N. *Langmuir* **1997**, *13*, 2171.
(38) Zhu, Z.; Sukhishivili, S. A. *J. Mater. Chem.* **2012**, *22*, 7667.
(39) Decher, G. *Science* **1997**, *277*, 132.
(40) Donath, E.; Sukhorukov, G. B.; Caruso, F.; Davis, S. A.; Mohwald, H. *Angew. Chem.* **1998**, *110*, 2323.
(41) Antipov, A. A.; Sukhorukov, G. B. *Adv. Colloid Interface Sci.* **2004**, *111*, 49.
(42) Pavlukhina, S.; Sukhishvili, S. *Adv. Drug Delivery Rev.* **2011**, *63*, 822.
(43) Bliznyuk, V. N.; Rinderspacher, F.; Tsukruk, V. V. *Polymer* **1998**, *39*, 5249.
(44) Tsukruk, V. V. *Adv. Mater.* **1998**, *10*, 253.
(45) Nguyen, R. M.; Zacharia, N. S.; Verploegen, E.; Hammond, P. T. *Chem. Mater.* **2007**, *19*, 5524.
(46) Khopade, A. J.; Caruso, F. *Nano Lett.* **2002**, *2*, 425.
(47) Khopade, A. J.; Caruso, F. *Biomacromolecules* **2002**, *3*, 1154.
(48) Kim, B.-S.; Lebedeva, O. V.; Kim, D. H.; Caminade, A.-M.; Majoral, J.-P.; Knoll, W.; Vinogradova, O. I. *Langmuir* **2005**, *21*, 7200.
(49) Kim, B.-S.; Lebedeva, O. V.; Koynov, K.; Gong, H.; Caminade, A.-M.; Majoral, J.-P.; Vinogradova, O. I. *Macromolecules* **2006**, *39*, 5479.
(50) Webber, G. B.; Wanless, E. J.; Armes, S. P.; Tang, Y.; Li, Y.; Biggs, S. *Adv. Mater.* **2004**, *16*, 1794.
(51) Biggs, S.; Sakai, K.; Addision, T.; Schmid, A.; Arms, S. P.; Vamvakaki, M.; Butun, V.; Webber, G. *Adv. Mater.* **2007**, *19*, 247.
(52) Cho, J.; Hong, J.; Char, K.; Caruso, F. *J. Am. Chem. Soc.* **2006**, *128*, 9935.
(53) Hong, J.; Bae, W. K.; Lee, H.; Oh, S.; Char, K.; Caruso, F. *Adv. Mater.* **2007**, *19*, 4363.
(54) Sakai, K.; Webber, G. B.; Vo, C.-D.; Wanless, E. J.; Vamvakai, M.; Butun, V.; Armes, S. P.; Biggs, S. *Langmuir* **2008**, *24*, 116.
(55) Zhu, Z.; Sukhishvili, S. A. *ACS Nano* **2009**, *3*, 3595.
(56) Tan, W. S.; Zhu, Z.; Sukhishvili, S. A.; Rubner, M. F.; Cohen, R. E. *Macromolecules* **2011**, *44*, 7767.
(57) Son, K. J.; Yoon, H.-J.; Kim, J.-H.; Jang, W.-D.; Lee, Y.; Koh, W.-G. *Angew. Chem., Int. Ed.* **2011**, *50*, 1.
(58) Ma, N.; Zhang, H.; Song, B.; Wang, Z.; Zhang, Xi. *Chem. Mater.* **2005**, *17*, 5065.
(59) Ma, N.; Wang, Y.; Wang, Z.; Zhang, Xi. *Langmuir* **2006**, *22*, 3906.
(60) Addison, T.; Cayre, O. J.; Biggs, S.; Armes, S. P.; York, D. *Langmuir* **2008**, *24*, 13328.
(61) Addison, T.; Cayre, O. J.; Biggs, S.; Arms, S. P.; York, D. *Langmuir* **2010**, *26*, 6281.
(62) Hong, J.; Cho, J.; Char, K. *J. Colloid Interface Sci.* **2011**, *364*, 112.
(63) Gorodyska, G.; Kiriy, A.; Minko, S.; Tsitsilianis, C.; Stamm, M. *Nano Lett.* **2003**, *3*, 365.
(64) Stepanek, M.; Matejicek, P.; Humpolickova, J.; Havrankova, J.; Podhajecka, K.; Spirkova, M.; Tuzar, Z.; Tsitsilianis, C.; Prochazka, K. *Polymer* **2005**, *46*, 10493.
(65) Tsitsilianis, C.; Chaumont, P.; Remmp, P. *Makromol. Chem.* **1990**, *191*, 2319.
(66) Tsitsilianis, C.; Voulgaris, D. *Macromol. Chem. Phys.* **1997**, *198*, 997.
(67) Sheller, N. B.; Petrash, S.; Foster, M. D.; Tsukruk, V. V. *Langmuir* **1998**, *14*, 4535.
(68) Shchepelina, O.; Kozlovskaya, V.; Singamaneni, S.; Kharlampieva, E.; Tsukruk, V. V. *J. Mater. Chem.* **2010**, *20*, 6587.
(69) Jiang, C.; Tsukruk, V. V. *Adv. Mater.* **2006**, *18*, 829.
(70) Tsukruk, V. V. *Rubber Chem. Technol.* **1997**, *70*, 430.
(71) McConney, M. E.; Singamaneni, S.; Tsukruk, V. V. *Polym. Rev.* **2010**, *50*, 235.
(72) Magonov, S. N.; Elings, V.; Whangbo, M. H. *Surf. Sci.* **1997**, *375*, L385.
(73) Wang, D.; Moses, D.; Bazan, G. C.; Heeger, A. J.; Lal, J. *J. Macromol. Sci., Pure Appl. Chem.* **2001**, *A38* (12), 1175.
(74) Zhao, J. K.; Gao, C. Y.; Liu, D. *J. Appl. Crystallogr.* **2010**, *43*, 1068.
(75) Wignall, G. D.; Bates, F. S. *J. Appl. Crystallogr.* **1987**, *20*, 28.
(76) Mauser, T.; Déjuganet, C.; Sukhorukov, G. B. *J. Phys. Chem. B* **2006**, *110*, 20246.
(77) Kiriy, A.; Gorodyska, G.; Minko, S.; Steamm, M.; Tsitsilianis, C. *Macromolecules* **2003**, *36*, 23.
(78) Lvov, Y.; Decher, G.; Moehwald, H. *Langmuir* **1993**, *9*, 481.

(79) Kozlovskaya, V.; Kharlampieva, E.; Drachuk, I.; Cheng, D.; Tsukruk, V. V. *Soft Matter* **2010**, *6*, 3596.
(80) Gao, C.; Leporatti, S.; Moya, S.; Donath, E.; Möhwald, H. *Langmuir* **2001**, *17*, 3491.
(81) Singamaneni, S.; McConney, M. E.; Tsukruk, V. V. *Adv. Mater.* **2010**, *22*, 1263.
(82) Singamaneni, S.; Tsukruk, V. V. *Soft Matter* **2010**, *6*, 5681.
(83) Dähne, L.; Peyratout, C. S. *Angew. Chem., Int. Ed.* **2004**, *43*, 3762.
(84) Köhler, K.; Shchukin, D. G.; Möhwald, H.; Sukhorukov, G. B. *J. Phys. Chem. B* **2005**, *109*, 18250.
(85) Köhler, K.; Shchukin, D. G.; Sukhorukov, G. B.; Möhwald, H. *Macromolecules* **2004**, *37*, 9546.
(86) Kim, J. Y.; DeRocher, J. P.; Mao, P.; Han, J.; Cohen, R. E.; Rubner, M. F. *Chem. Mater.* **2010**, *22*, 6409.
(87) Leporatti, S.; Voigt, A.; Mitlöhner, R.; Sukhorukov, G.; Donath, E.; Möhwald, H. *Langmuir* **2000**, *16*, 4059.
(88) Gao, C.; Leporatti, S.; Donath, E.; Mohwald, H. *J. Phys. Chem. B* **2000**, *104*, 7144.
(89) Smith, E. G.; Webber, G. B.; Sakai, K.; Biggs, S.; Armes, S. P.; Wanless, E. J. *J. Phys. Chem. B* **2007**, *111*, 5536.
(90) Decher, G.; Lvov, Y.; Schmitt, J. *Thin Solid Fims* **1994**, *244*, 772.
(91) Sukhorukov, G. B.; Schmitt, J.; Decher, G. *Ber. Bunsen-Ges. Phys. Chem.* **1996**, *100*, 948.
(92) Dubas, S.; Schlenoff, J. B. *Langmuir* **2001**, *17*, 7725.
(93) Armstrong, J. K.; Wenby, R. B.; Meiselman, H. J.; Fisher, T. C. *Biophys. J.* **2004**, *87*, 4259.
(94) Shchepelina, O.; Drachuk, I.; Gupta, M. K.; Lin, J.; Tsukruk, V. V. *Adv. Mater.* **2011**, *23*, 4655.
(95) Freltoft, T.; Kjems, J. K.; Sinha, S. K. *Phys. Rev. B* **1986**, *33*, 269.
(96) Schmidt, P. W. *J. Appl. Crystallogr.* **1991**, *24*, 414.
(97) Zimnitsky, D.; Shevchenko, V. V.; Tsukruk, V. V. *Langmuir* **2008**, *24*, 5996.
(98) Tsukruk, V. V.; Bliznyuk, V. N.; Visser, D. W.; Campbell, A. L.; Bunning, T.; Adams, W. W. *Macromolecules* **1997**, *30*, 6615.
(99) Tsukruk, V. V. *Prog. Polym. Sci.* **1997**, *22*, 247.
(100) Debye, P.; Bueche, A. M. *J. Appl. Phys.* **1949**, *20*, 518.
(101) Debye, P.; Anderson, H. R.; Brumberger, H. *J. Appl. Phys.* **1957**, *28*, 679.